

Safe Navigation in Dynamic Environments using Density Functions

Sriram S. K. S. Narayanan, Joseph Moyalan, and Umesh Vaidya

Abstract—This work uses density functions for safe navigation in dynamic environments. The dynamic environment consists of time-varying obstacles as well as time-varying target sets. We propose an analytical construction of time-varying density functions to solve these navigation problems. The proposed approach leads to a time-varying feedback controller obtained as a positive gradient of the density function. This paper's main contribution is providing convergence proof using the analytically constructed density function for safe navigation in the presence of a dynamic obstacle set and time-varying target set. The results are the first of this kind developed for a system with integrator dynamics and open up the possibility for application to systems with more complex dynamics using methods based on control density function and inverse kinematic-based control design. We present the application of the developed approach for collision avoidance in multi-agent systems and robotic systems. While the theoretical results are produced for first-order integrator systems, we demonstrate how the framework can be applied for systems with non-trivial dynamics, such as Dubin's car model and fully actuated Euler-Lagrange system with robotics applications.

I. INTRODUCTION

Safe navigation in dynamic environments is a fundamental challenge in robotics and autonomous systems [1], [2]. The objective is to find a safe trajectory that the system must follow to reach a target (or track a target trajectory) while avoiding dynamic obstacles. Over the years, several methodologies have been developed to address these challenges effectively, such as sample-based methods, gradient-based methods, optimization-based methods, and reachable set computations [3].

Sample-based algorithms like Rapidly-exploring Random Trees (RRT) and Probabilistic Roadmaps (PRM) are widely used in navigation problems due to their flexibility and efficiency in high-dimensional spaces. RRT* introduced optimality by ensuring asymptotic convergence to the best possible path, while extensions like RRT-Connect improve speed and scalability. The effectiveness of these methods for dynamic environments has been studied in [4]–[6]. However, they do not provide any safety guarantees.

Gradient-based methods are praised for their computational speed and suitability for real-time applications. Still, they may require careful tuning of parameters and cost functions to

ensure effectiveness and safety in complex, dynamic scenarios. These methods often use potential fields where attractive forces guide the robot toward the goal and repulsive forces push it away from obstacles. The Artificial Potential Field (APF) approach introduced in [7] is a seminal work in this domain, enabling real-time obstacle avoidance through the computation of artificial forces. Despite their simplicity and computational efficiency, APF methods are prone to issues such as local minima and oscillations in dynamic environments. To address these shortcomings, subsequent works have proposed enhancements like the Virtual Force Field (VFF) [8] and the Navigation Function approach [9]. Navigation functions are topologically constructed to provide safety and convergence guarantees, but limitations exist on the possible construction of navigation functions through the limited diffeomorphic mapping to a sphere world. Under dynamic environmental constraints, [10], [11] formally extended navigation functions to time-varying targets. Next, the social force model (SFM) [12] was originally developed to simulate pedestrian dynamics. This model treats pedestrians as particles influenced by social forces, including attraction to the goal and repulsion from obstacles and other pedestrians. The Social Force Model has been extended to various robotic applications, particularly in environments where human-robot interactions are prominent [13].

In recent years, Control Barrier Function (CBF) methods have emerged as a powerful approach for ensuring safety in dynamic environments [14]–[16]. In [17], CBFs combined with Control Lyapunov Functions (CLFs) in quadratic programs were used to manage nonholonomic mobile robots navigating through dynamic obstacles. Their work highlights how CBFs can enforce safety constraints in real-time, ensuring collision avoidance while maintaining desirable robot performance. Similarly, [18]–[20] explores multiagent systems where CBF-based controllers are employed to address the collision avoidance problem. They provide insights into how CBFs can be adapted for complex multiagent scenarios, ensuring safety guarantees even under challenging conditions. These studies underscore the versatility and robustness of CBFs for safe navigation, demonstrating their potential for real-world applications involving dynamic obstacles and multiple interacting agents. While CBFs ensure safety, they do not guarantee convergence, making it necessary to augment them with CLFs to achieve both safety and stability. Finding suitable Lyapunov functions can be challenging. Further, constructing CBFs is not trivial, as it requires careful design to account for system dynamics and safety constraints [21].

Financial support from the NSF CPS award 1932458 and NSF 2031573 is greatly acknowledged. Sriram S. K. S. Narayanan, Joseph Moyalan, and Umesh Vaidya are with the Department of Mechanical Engineering, Clemson University, Clemson, SC; email: {sriramk, jmoyala, uvaidya}@clemson.edu.

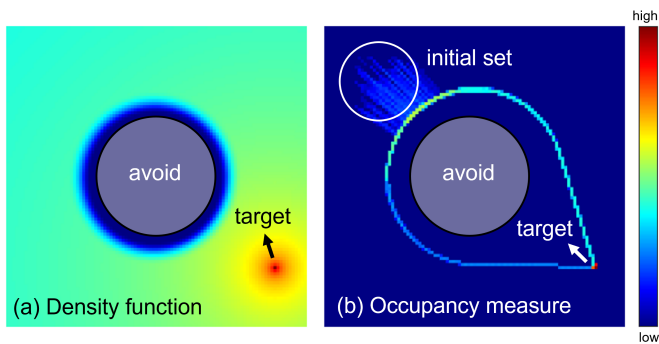


Fig. 1. (a) Density function defined on an environment with a circular unsafe set and a point target, (b) Corresponding occupancy measure obtained using trajectories from 100 initial conditions sampled within the initial set. (color bar is in log scale)

Reachability-based methods play a crucial role in ensuring safe navigation in dynamic environments by precomputing the set of all states a system can reach within a given time frame. Hamilton-Jacobi (HJ) reachability analysis is a verification method that computes the reach-avoid set, which encompasses the states from which a system can safely reach a target while adhering to time-varying constraints [22]. This approach has been effectively applied in various contexts. For instance, [23] demonstrated its utility in stochastic environments, combining HJ reachability with potential fields for dynamic obstacle avoidance. Moreover, [24] and [25] refined these methods for efficient path planning and provably safe navigation in uncertain environments. Recent advancements, such as multi-time reachability by [26], further enhance its applicability in complex scenarios with time-varying obstacles and constraints. These studies underscore the versatility and efficiency of HJ reachability in addressing safety and navigation challenges in dynamic environments. However, computing reachable sets can be computationally expensive for large-dimension systems. Although HJ-reachability is optimal, providing safety guarantees is nontrivial. In contrast, the density-based approach proposed in this work leads to a feedback controller that prioritizes safety over optimality and can be scaled easily for high-dimensional systems.

Alternatively, the navigation problem can be formulated in the dual space of density. It has been shown that density functions can be jointly viewed as both a safety certificate and a weaker notion of convergence, enabling the synthesis of safe controllers for navigation. [27]–[30]. [31] introduced a convex formulation using the navigation measure to synthesize safe controllers for the navigation problem. These works were extended to data-driven methods using linear transfer operators for navigation under safety constraints [32]–[34]. More recently, [35] proposed an analytically constructed density function to synthesize a controller that jointly solves the obstacle avoidance and convergence problem [35]. By having a physically intuitive interpretation of occupation through density and, therefore, navigation, [35] was able to exploit this to design an analytical feedback controller that solves the almost everywhere navigation (a.e.) problem.

The main contributions of this work are outlined below. We provide an analytical construction of density functions for time-varying obstacles (with static targets) and time-varying target trajectories (with static obstacles). We provide a feedback controller with theoretical safety guarantees and almost everywhere convergence for both cases using the analytically constructed density function. To the best of the author’s knowledge, this is the first rigorous convergence proof for the time-varying unsafe case. We demonstrate the application of the developed framework on density-based safe control design for multi-agent collision avoidance and safe trajectory tracking for robotic systems.

The rest of the paper is organized as follows. In Section II, we introduce the preliminaries and illustrate the use of density functions for a.e. navigation in static environments. In Section III, we introduce the problem statements and provide the main results for a.e. safe navigation in dynamic environments. Specifically, we provide theorems to guarantee safety under dynamic obstacles (with static targets) and dynamic targets (with static obstacles). In Section IV, we show applications of the proposed approach with a single integrator system in dynamic environments, multi-agent collision avoidance (with comparisons to the social force model), and safe trajectory tracking for a two-link planar robotic arm. Finally, in Section V, we provide concluding remarks for this work.

II. PRELIMINARIES AND NOTATIONS

Notations: We use \mathbb{R}^n to denote the n dimensional Euclidean space. $\mathbf{x} \in \mathbb{R}^n$ denotes a vector of system states, $\mathbf{u} \in \mathbb{R}^m$ is a vector of control inputs. Let $\mathbf{X} \subset \mathbb{R}^n$ be a bounded subset that denotes the workspace for the robot. \mathbf{X}_0 , \mathbf{X}_T , $\mathbf{X}_{u_k} \subset \mathbf{X}$, for $k = 1, \dots, L$ denote the initial, target, and unsafe sets, respectively. Next, we use $\mathbf{x}_T \in \mathbf{X}_T$ to denote a static target point and $\mathbf{x}_T(t)$ to denote the trajectory of a time-varying target. For simplicity, we assume $\mathbf{x}_T = 0$ for static target scenarios. $\mathbf{X}_u = \cup_{k=1}^L \mathbf{X}_{u_k}$ defines the unsafe set and $\mathbf{X}_s := \mathbf{X} \setminus \mathbf{X}_u$ defines the safe set. We use $\mathcal{C}^k(\mathbf{X})$ to denote the space of all k -times differentiable functions of \mathbf{x} . We define the set $\mathbf{X}_1 := \mathbf{X} \setminus \mathcal{B}_\delta$, where \mathcal{B}_δ is the δ neighborhood of the origin for arbitrary small δ . We use $\mathcal{M}(\mathbf{X})$ to denote the space of all measures on \mathbf{X} and $m(\cdot)$ to denote the Lebesgue measure. $\mathbb{1}_A(\mathbf{x})$ denotes the indicator function for set $A \subset \mathbf{X}$. Further, let $\|\mathbf{x}\|$ denote the 2-norm of a vector \mathbf{x} .

Density functions are a physically intuitive way to solve almost everywhere (a.e.) safe navigation (with respect to the Lebesgue measure) presented in Problem 1. In this paper, we define safe trajectories for a system as the ones that have zero occupancy in the unsafe set \mathbf{X}_u . The formal definition of occupancy used in this paper is defined below.

Definition 1: (Occupancy of a set) Let $\mathbf{A} \subset \mathbf{X}$ be a measurable set. The occupancy of the system trajectories $\mathbf{x}(t)$ with initial condition \mathbf{x} , in the set \mathbf{A} while traversing from the initial set $\mathbf{X}_0 \ni \mathbf{x}$ to the target set \mathbf{X}_T is defined as

$$\mu(\mathbf{A}) := \int_0^\infty \int_{\mathbf{X}} \mathbb{1}_{\mathbf{A}}(\mathbf{x}(t)) \mathbb{1}_{\mathbf{X}_0}(\mathbf{x}) d\mathbf{x} dt \quad (1)$$

The occupancy measure as defined in (1) was introduced in [31] as a *navigation measure* for solving a.e. navigation

problem for a discrete-time dynamical system. Using the physical interpretation of occupancy, it follows that if the measure is zero on a particular set, then that set will not be occupied and hence traversed by the system trajectories. Under the assumption, that the measure is continuous w.r.t. Lebesgue, then following the Radon–Nikodym theorem, one can define a density function. The construction of such a density function for safe navigation in a dynamic environment is the focus of this paper.

In Fig 1a. we show a plot of such a density function and the associated dynamics induced by the density function. We see that the system trajectories have zero occupancy on the unsafe set \mathbf{X}_u and a maximum occupancy in the target set \mathbf{X}_T . So, by ensuring that the navigation density is zero on the unsafe set and maximum at the target set, it is possible to induce dynamics whereby the system trajectories will reach the desired target set while avoiding the unsafe set. We exploit this occupancy-based interpretation in the construction of analytical density functions for navigation in a dynamic environment consisting of time-varying obstacles and targets set in Section III-A.

Definition 2: [Almost everywhere (a.e.) stability] The target set \mathbf{X}_T of the system is said to be a.e. stable w.r.t. measure $\mu_0 \in \mathcal{M}(\mathbf{X})$ if

$$\mu_0\{\mathbf{x} \in \mathbf{X} : \lim_{t \rightarrow \infty} \mathbf{x}(t) \notin \mathbf{X}_T\} = 0. \quad (2)$$

A. Safe Navigation with Static Obstacles and Static Target

In [35], an analytical construction of density function, $\rho(\mathbf{x})$, was provided for safe navigation in an environment consisting of static obstacle sets. Specifically, the density function proposed in [35] can be used for obstacle avoidance while also satisfying the convergence to the target set properties. For a 2D single integrator system defined by $\dot{\mathbf{x}} = \mathbf{u}$, the control law given by the positive gradient of the density function, i.e., $\mathbf{u} = \nabla \rho(\mathbf{x})$ will guarantee almost everywhere (a.e.) safe navigation, i.e., the system trajectories will converge to the target set \mathbf{X}_T while avoiding the unsafe set \mathbf{X}_u . We provide an example to demonstrate the convergence and avoidance properties of such a controller.

Example 1 (Static Unsafe Set and Target): Consider the integrator dynamics $\dot{\mathbf{x}} = \mathbf{u}$ with control law $\mathbf{u} = \nabla \rho(\mathbf{x})$ (i.e., positive gradient of density function). The environment is defined with the target set at $\mathbf{x}_T = [10, 0]$ with three circular unsafe sets \mathbf{X}_{u_1} , \mathbf{X}_{u_2} and \mathbf{X}_{u_3} each with radius $r = 1$. The radius of the sensing region for each obstacle is given by s_k as shown in Fig. 2a. Note that we show two solution trajectories obtained with $s_{k_1} = 2$ and $s_{k_2} = 2.5$ respectively. It can be seen that both trajectories to the target while avoiding unsafe sets.

Fig. 2b shows the value of the density function $\rho(\mathbf{x})$ along the solution trajectory. Note that $\rho(\mathbf{x}) > \theta > 0 \forall t$, i.e., the trajectories never enter the unsafe set as $\rho(\mathbf{x}) = 0$ on the unsafe set. Further, $\rho(\mathbf{x})$ is the maximum near the target. This matches with the occupancy-based interpretation of density functions provided in [35]. The main contribution of this work is to provide the solution to a.e. safe navigation problem in

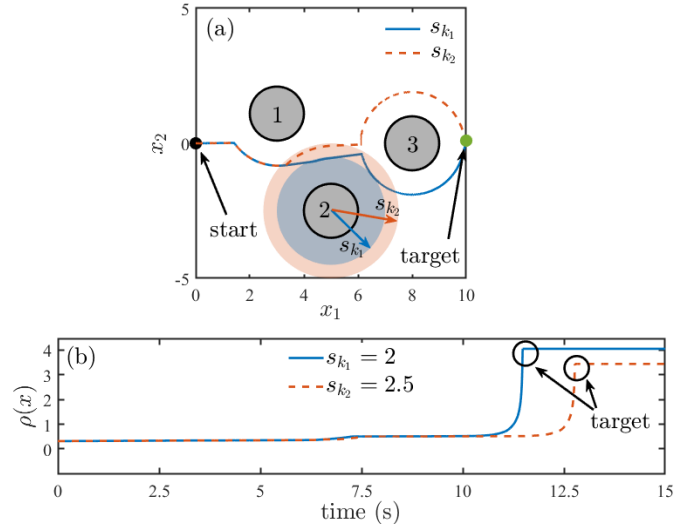


Fig. 2. **Static Unsafe Set and Target:** (a) Solution trajectory (red) obtained using the density-based controller and (b) the corresponding value of $\rho(\mathbf{x})$.

a dynamic environment consisting of time-varying obstacles and target sets. Furthermore, we demonstrate the application of the developed framework for multi-agent a.e. safe navigation problems.

III. DYNAMIC ALMOST EVERYWHERE SAFE NAVIGATION

In this section, we define the safe navigation problem with time-varying unsafe and target set.

Problem 1 (Dynamic Almost Everywhere Safe Navigation): Consider the first-order integrator dynamics of the form

$$\dot{\mathbf{x}} = \mathbf{u}. \quad (3)$$

The objective is to design a feedback control input $\mathbf{u} = \mathbf{k}(t, \mathbf{x})$, possibly time-varying, to drive the trajectories of (3) from a.e.¹ (w.r.t. Lebesgue measure) initial condition from the initial set \mathbf{X}_0 to a time-varying target set \mathbf{x}_T while avoiding time-varying unsafe set \mathbf{X}_{u_k} for $k = 1, \dots, L$. We assume that either the unsafe sets $\mathbf{X}_{u_k}(t)$ or $\mathbf{x}_T(t)$ are time-varying.

Remark 1: While the results are developed for first-order integrator dynamics, in our simulation section, we demonstrate how the results can be generalized to important classes of dynamics that arise in robotics applications such as Dubin’s car model and for systems for which controller can be designed using inverse kinematics.

Assumption 1: In the construction of the density function for a.e. navigation in a dynamic environment, it is assumed that the controller has information about the time-varying unsafe and target set.

Remark 2: While the theoretical results are developed for the case where the complete information of the dynamic environment is available in the construction of density function, we will demonstrate through the simulation example how

¹In the rest of the paper it is implicitly assumed that a.e. is w.r.t. Lebesgue measure unless stated otherwise.

the theory can be applied for the cases where only local information is available.

A. Construction of Time-varying Density Functions

We exploit the occupancy-based interpretation of density in constructing analytical expressions for time-varying density functions. For each time-varying obstacle k , we start with constructing the unsafe set $\mathbf{X}_{u_k}(t)$, where the boundary of the unsafe set is described in terms of the zero-level set of a function. Let $h_k(t, \mathbf{x}) : \mathbb{R}^n \rightarrow \mathbb{R}$ be a continuous scalar-valued function for $k = 1, \dots, L$ such that the set $\{\mathbf{x} \in \mathbf{X} : h_k(t, \mathbf{x}) = 0\}$ defines the boundary of each unsafe set \mathbf{X}_{u_k} . Thus, the unsafe set $\mathbf{X}_{u_k}(t)$ is defined as follows

$$\mathbf{X}_{u_k}(t) := \{\mathbf{x} \in \mathbf{X} : h_k(t, \mathbf{x}) \leq 0\}. \quad (4)$$

For a well-defined obstacle set, we assume that the level set of $h_k(t, \mathbf{x})$ is connected. For example, a circular obstacle with center at \mathbf{c}_k and radius r_k , the unsafe set $\mathbf{X}_{u_k}(t)$ is defined as

$$\mathbf{X}_{u_k}(t) = \{\mathbf{x} \in \mathbf{X} : \|\mathbf{x} - \mathbf{c}_k(t)\| \leq r_k\}. \quad (5)$$

Next, for each obstacle, we define a sensing region $\mathbf{X}_{s_k}(t)$ with radius s_k that encloses the unsafe set $\mathbf{X}_{u_k}(t)$. Inside this region, the robot starts to react to the unsafe set. Let $s_k(t, \mathbf{x}) : \mathbb{R}^n \rightarrow \mathbb{R}$ be a continuous scalar-valued function for $k = 1, \dots, L$ such that the set $\{\mathbf{x} \in \mathbf{X} : s_k(t, \mathbf{x}) = 0\}$ defines the boundary of this sensing region. Then, the sensing region can be defined as

$$\mathbf{X}_{s_k}(t) := \{\mathbf{x} \in \mathbf{X} : s_k(t, \mathbf{x}) \leq 0\} \setminus \mathbf{X}_{u_k}(t). \quad (6)$$

Again we assume that the level set of the function $s_k(t, \mathbf{x})$ is connected. A circular sensing region for circular unsafe sets can be defined as

$$\mathbf{X}_{s_k}(t) = \{\mathbf{x} \in \mathbf{X} : \|\mathbf{x} - \mathbf{c}_k(t)\| \leq s_k\} \setminus \mathbf{X}_{u_k}(t). \quad (7)$$

This sensing region plays a crucial role in extending the proposed framework where global information about the unsafe is assumed to be available in the case when only local information inside the sensing region is used for safe navigation.

Next, we define an inverse bump function $\Psi_k(t, \mathbf{x})$, which is a smooth \mathcal{C}^∞ function that captures the geometry of the unsafe set $\mathbf{X}_{u_k}(t)$ and can be constructed using the following sequence of functions. We first define an elementary \mathcal{C}^∞ function f as follows [36]

$$f(\tau) = \begin{cases} \exp\left(\frac{-1}{\tau}\right), & \tau > 0 \\ 0, & \tau \leq 0 \end{cases}$$

where $\tau \in \mathbb{R}$. Next, we construct a smooth version of a step function \bar{f} from f as follows

$$\bar{f}(\tau) = \frac{(1 - \theta)f(\tau)}{f(\tau) + f(1 - \tau)} + \theta \quad (8)$$

To incorporate the geometry of $\mathbf{X}_{u_k}(t)$ and $\mathbf{X}_{s_k}(t)$, we define a change of variables such that

$$\phi_k(\mathbf{x} - \mathbf{c}_k(t)) = \bar{f}\left(\frac{\|\mathbf{x} - \mathbf{c}_k(t)\|^2 - r_k^2}{s_k^2 - r_k^2}\right). \quad (9)$$

The resulting function $\Phi_k(t, \mathbf{x})$ take the following form,

$$\Psi_k(\mathbf{x} - \mathbf{c}_k(t)) := \begin{cases} \theta, & \mathbf{x} \in \mathbf{X}_{u_k}(t) \\ \phi_k(\mathbf{x} - \mathbf{c}_k(t)), & \mathbf{x} \in \mathbf{X}_{s_k}(t) \\ 1, & \text{otherwise} \end{cases}. \quad (10)$$

Remark 3: For notation convenience, we will simply write $\Psi_k(\mathbf{x} - \mathbf{c}_k(t))$ as $\Psi_k(t, \mathbf{x})$, however later in the proof of one of the main results, we will use this specific form of the inverse bump function $\Psi_k(t, \mathbf{x})$. When \mathbf{x} is outside the sensing region, i.e., $\mathbf{x} \notin \mathbf{X}_{s_k}$, we have $\Psi = 1$ and hence both the first and second derivatives of Ψ w.r.t. \mathbf{x} are zero. Further, $\Psi_k(\mathbf{x}, t)$ makes a smooth transition from $0 < \theta \ll 1$ to 1 inside the sensing region. α , θ , and s_k are scalar tuning parameters that can be used to obtain trajectories with the desired behavior.

The above construction of function Ψ_k is used to ensure that the system trajectory will have zero occupancy on the unsafe set. To ensure that the system dynamics are attracted to the target set, we introduce a distance function, $V(\mathbf{x})$. The distance function can be chosen to adapt to the geometry of the underlying configuration space of the system. For a Euclidean space with $\mathbf{x} \in \mathbb{R}^n$, we pick $V(\mathbf{x}) = \|\mathbf{x}\|^2$ (since the target is assumed to be at the origin). Note that in Euclidean space, the simple distance function will work as the dynamics are assumed to be integrators. The construction of an appropriate distance function for the system with drift remains a challenge but is not the focus of this paper. We define a density function for safe navigation with time-varying unsafe sets as follows.

Definition 3 (Dynamic unsafe set and static target set):

The navigation density function for the case of dynamic unsafe set and static target set is defined as

$$\rho_o(t, \mathbf{x}) = \frac{\prod_{k=1}^L \Psi_k(t, \mathbf{x})}{(V(\mathbf{x}) + \kappa)^\alpha} = \frac{\Psi(t, \mathbf{x})}{V_1(\mathbf{x})^\alpha}. \quad (11)$$

where $V_1(\mathbf{x}) = V(\mathbf{x}) + \kappa$ for some constant $\kappa > 0$ to ensure that the denominator is bounded away from zero.

For representing dynamic target sets, we next introduce a distance function, $V(t, \mathbf{x})$, which measures the distance from \mathbf{x} to the target set. The explicit time dependence of the distance function V reflects the fact that the target set could be dynamic. For a Euclidean space with $\mathbf{x} \in \mathbb{R}^n$, we pick $V(t, \mathbf{x}) = \|\mathbf{x} - \mathbf{x}_T(t)\|^2$, where $\mathbf{x}_T(t)$ is the known dynamics of the target set.

Definition 4 (Dynamic target set and static unsafe set):

The navigation density function for this case is defined as

$$\rho_T(t, \mathbf{x}) = \frac{\prod_{k=1}^L \Psi_k(\mathbf{x})}{(V(t, \mathbf{x}) + \kappa)^\alpha} = \frac{\Psi(\mathbf{x})}{V_1(t, \mathbf{x})^\alpha}. \quad (12)$$

where $V_1(t, \mathbf{x}) = V(t, \mathbf{x}) + \kappa$ for some constant $\kappa > 0$. Here, $\Psi_k(\mathbf{x})$ is as given in 10 with $\mathbf{c}_k(t)$ replaced with \mathbf{c}_k a constant independent of time.

The construction of this density function consists of two parts. The $\Psi(t, \mathbf{x})$ or $\Psi(\mathbf{x})$ captures the information of the unsafe set, and $V(\mathbf{x})$ encodes the information of the target set. The function $\Psi(t, \mathbf{x})$ is essentially a zero one function, taking small value θ inside the unsafe set and making a smooth transition from θ to one within the sensing region. This is crucial as this means that the information about the unsafe set is not known globally but only inside the sensing region

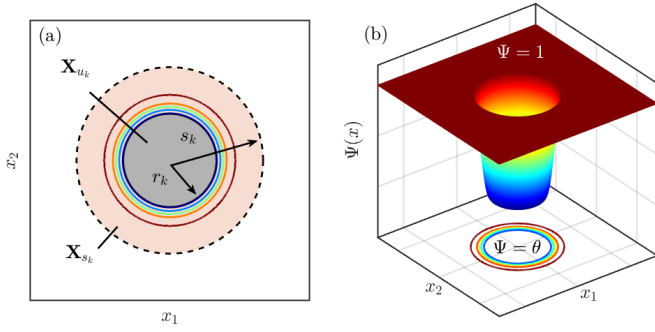


Fig. 3. Inverse bump function $\Psi(\mathbf{x})$ (a) top view showing contours and (b) 3D view.

(6). This observation is crucial when we demonstrate the application of the developed framework for collision avoidance in multi-agent systems with local information of the other agents (see Section IV-B).

Remark 4: Static unsafe set and static target set will be the special case of the construction procedure outlined above. In particular, for the case when the unsafe set is static, $\mathbf{c}_k(t)$ can be replaced with \mathbf{c}_k (i.e., independent of time), signifying the center of the unsafe set. Similarly, the static target set will be the special case of the time-varying target case.

Next, we make the following assumptions.

Assumption 2:

1. We assume that the distance between the initial set, the unsafe sets, and the target set are all bounded away from zero by some positive constant.
2. We assume that the obstacle sets \mathbf{X}_{u_k} for $k = 1, \dots, L$ are inside the bounded subset of \mathbf{X}_1 .
3. For time-varying obstacle case, we assume that for all $k = 1, \dots, L$, $c_k(t)$ and $\dot{c}_k(t)$ are continuous and bounded functions for all $t \geq 0$.
4. In the sensing region, i.e., $\mathbf{x} \in \mathbf{X}_{s_k}$, we assume the following uniform bounds independent of \mathbf{x} and for all $t \geq 0$.

$$\left| \frac{\partial \Psi}{\partial t} \right| \leq c_{\Psi_t}$$

$$\left| \frac{\partial \Psi}{\partial x_j} \right| \leq \bar{c}_{\Psi_{x_j}}, \quad \left| \frac{\partial^2 \Psi}{\partial x_j^2} \right| \leq \bar{c}_{\Psi_{x_j^2}}, \quad j = 1, \dots, n.$$

5. For all $\mathbf{x} \in \mathbf{X}_1$, and for all $t \geq 0$, we assume

$$\frac{\partial^2 V}{\partial x_j^2} \leq \bar{d}_{V_{x_j^2}}, \quad d_V \|\mathbf{x}\|^2 \leq V \leq \bar{d}_V \|\mathbf{x}\|^2,$$

$$d_{V_x} \|\mathbf{x}\| \leq \left| \frac{\partial V}{\partial x_j} \right| \leq \bar{d}_{V_x} \|\mathbf{x}\|, \quad j = 1, \dots, n.$$

6. For time-varying target case, we assume that $\mathbf{x}_T(t)$ and $\dot{\mathbf{x}}_T(t)$ are continuous and bounded functions for all $t \geq 0$.

Remark 5: The uniform bounds on the function Ψ in the sensing region can be assumed as all the obstacle sets and hence the sensing region is bounded. Furthermore, the function Ψ makes a smooth transition from θ to one. Similarly, the

bounds on the distance function V assume that the distance function is bounded from above and below by a quadratic function of \mathbf{x} .

B. Dynamic Almost Everywhere Safe Navigation using Time-varying Density Functions

In this section, we prove the main results of this paper on the convergence proof for the dynamic unsafe and target set with the proposed construction of density functions in Eqs. (11) and (12) respectively.

1) *Dynamic Unsafe Set:* Given the construction of $\rho_o(t, \mathbf{x})$ in (11) for dynamic unsafe set, we design a controller $\mathbf{u} = \mathbf{k}(t, \mathbf{x})$ as the positive gradient of $\rho_o(t, \mathbf{x})$, i.e.,

$$\begin{aligned} \dot{\mathbf{x}} &= \mathbf{k}(t, \mathbf{x}) = \beta \nabla \rho_o(t, \mathbf{x}) \\ &= \beta \left(-\frac{\alpha}{V_1^{\alpha+1}} \frac{\partial V}{\partial \mathbf{x}} \prod_{k=1}^L \Psi_k(t, \mathbf{x}) + \frac{1}{V_1^\alpha} \frac{\partial}{\partial \mathbf{x}} \prod_{k=1}^L \Psi_k(t, \mathbf{x}) \right)^\top. \end{aligned} \quad (13)$$

where β is a positive constant and ρ_o is as given in Eq. (11). The role of the positive constants β and α will be clarified in the proof of the main theorems of this paper.

Remark 6: The system dynamics for the dynamic unsafe set given by (13) is locally asymptotically stable. Following Assumption 2.1, the system dynamics in the small neighborhood of the origin for a time-varying unsafe set is reduced to

$$\dot{\mathbf{x}} = \beta \left(-\frac{\alpha}{V_1(\mathbf{x})^{\alpha+1}} \frac{\partial V}{\partial \mathbf{x}} \right)^\top.$$

Let $V(\mathbf{x})$, the distance function be the Lyapunov function, we have

$$\dot{V} = \frac{\partial V}{\partial \mathbf{x}} \beta \left(-\frac{\alpha}{V_1^{\alpha+1}} \frac{\partial V}{\partial \mathbf{x}} \right)^\top < 0$$

The local stability then follows using results from [37]. With no loss of generality, we can assume that the B_δ is a neighborhood of the origin where the system is locally stable.

The following theorem shows the results for safe navigation with a dynamic unsafe set.

Theorem 1 (Dynamic Unsafe Set): Under Assumption 2, there exists α , β and θ such that the dynamical system given in (13) with the density function defined in equation (11) will solve the a.e. navigation problem as stated in Problem 1 with time-varying unsafe sets and static target sets.

Proof: The proof of this theorem is included in the Appendix. ■

2) *Dynamic Target Set:* Similarly, for tracking the time-varying target in the presence of static unsafe sets we proposed the following dynamics.

$$\dot{\mathbf{x}} = \mathbf{k}(\mathbf{x}, t) = \beta \nabla \rho_T(t, \mathbf{x}) + \dot{\mathbf{x}}_T(t) \quad (14)$$

where again ρ_T is as defined in Eq. (12) and β is a positive constant. Notice that for the time-varying target case, we have system dynamics forced by $\dot{\mathbf{x}}_T(t)$.

Remark 7: The closed-loop system in (14) will asymptotically track the target trajectory, $\mathbf{x}_T(t)$ for all initial condition

\mathbf{x} in the small neighborhood of $\mathbf{x}_T(t)$. Again following Assumption 2.1, the system dynamics in the small neighborhood of $\mathbf{x}_T(t)$ for a time-varying target case is reduced to

$$\begin{aligned}\dot{\mathbf{x}} &= \beta \left(-\frac{\alpha}{V_1(\mathbf{x})^{\alpha+1}} \frac{\partial V}{\partial \mathbf{x}} \right) + \dot{\mathbf{x}}_T \\ &= -\frac{2\alpha\beta}{(\|\mathbf{x} - \mathbf{x}_T\|^2 + \kappa)^{\alpha+1}} (\mathbf{x} - \mathbf{x}_T) + \dot{\mathbf{x}}_T\end{aligned}\quad (15)$$

substituting $e = \mathbf{x} - \mathbf{x}_T$ and $\dot{e} = \dot{\mathbf{x}} - \dot{\mathbf{x}}_T$ in (15), we get

$$\dot{e} = -K_p e \quad (16)$$

where

$$K_p = \frac{2\alpha\beta}{(\|e\|^2 + \kappa)^{\alpha+1}}.$$

Since K_p is uniformly bounded away from zero, we can conclude from (16) that $e \rightarrow 0$ as $t \rightarrow \infty$. Therefore, the solution of the closed-loop system in (14) will track the desired trajectory \mathbf{x}_T for all initial conditions starting inside the small neighborhood of \mathbf{x}_T .

The following theorem shows the results for safe navigation with a dynamic target set.

Theorem 2 (Dynamic Target Set): Under Assumption 2, there exists α , β and θ such that the dynamical system given in (14) with the density function defined in equation (12) will solve the a.e. navigation problem as stated in Problem 1 with static unsafe sets and time-varying target sets.

Proof: Consider the change of coordinates given by $\mathbf{y}(t) = \mathbf{x} - \mathbf{x}_T(t)$ for the time-varying target case system in (14). Therefore,

$$\dot{\mathbf{y}} = \beta \nabla \rho_T(t, \mathbf{y} + \mathbf{x}_T(t)) \quad (17)$$

Now recalling the definition of $\rho_T(t, \mathbf{x})$ and using the fact that $V(\mathbf{x}, t) = \|\mathbf{x} - \mathbf{x}_T(t)\|^2$, it follows that

$$\rho_T(t, \mathbf{y} + \mathbf{x}_T(t)) = \frac{\Psi(\mathbf{y} + \mathbf{x}_T(t))}{V(\mathbf{y})^\alpha} \quad (18)$$

Now, recalling Remark 3, we can rewrite (18) as follows:

$$\begin{aligned}\rho_T(t, \mathbf{y} + \mathbf{x}_T(t)) &= \frac{\Psi(\mathbf{y} - (-\mathbf{x}_T(t)))}{V(\mathbf{y})^\alpha} \\ &= \rho_o(t, \mathbf{y})\end{aligned}$$

Therefore, we can rewrite (17) as follows:

$$\dot{\mathbf{y}} = \beta \nabla \rho_o(t, \mathbf{y}) \quad (19)$$

Now, using Theorem 1 for (19), we can show that the solution of (19) will converge to the target at the origin in the \mathbf{y} -coordinates while avoiding unsafe sets. This ensures that the solution of (14) will converge to $\mathbf{x}_T(t)$ in the \mathbf{x} -coordinates while avoiding unsafe sets. Similarly, since $\mathbf{y} \in \mathbf{X}_1$ for all $t \geq 0$ (Assumption 2.5), the appropriate range of α and β are given by (54) and (59) respectively. ■

IV. SIMULATIONS RESULTS

In this section, we present simulation results to verify the theoretical framework developed in this paper. All the simulations are conducted on an Intel Core i9-12900K CPU and 32 GB of RAM with a simulation timestep of 0.1 s. Implementation details can be found at https://github.com/sriram-2502/time_varying_density

A. Dynamic Unsafe Set

The first example is for time-varying obstacle sets. Given the initial condition $\mathbf{X}_0 = [0, 0]$ and a static target $\mathbf{x}_T = [10, 0]$, the objective is to converge to the target while avoiding time-varying unsafe sets (\mathbf{X}_{u_k} for $k = 1, \dots, 4$). The trajectory of the center $\mathbf{c}_k(t)$ of each obstacle is defined as follows

$$\begin{aligned}c_1(t) &= [2, 0.25t], & c_2(t) &= [4, 7 - 0.2t] \\ c_3(t) &= [6 + 0.1 \sin(t), 0.15t - 6], & c_4(t) &= [8, 5 - 0.12t].\end{aligned}$$

Each obstacle is modeled as a circular disk with a radius $r_k = 0.75$ with the sensing radius of $s_k = 1.5$ as defined in (5) and (7) respectively. We use Theorem 1 to define the density-based controller for this system. For this example we add input constraints, $\mathbf{u} \in [-\mathbf{u}_{\max}, \mathbf{u}_{\max}]$ where \mathbf{u}_{\max} is the bound on control. Without formality, we constrain the control when $\|\mathbf{u}\|_\infty > \mathbf{u}_{\max}$ by normalizing the control as $\left(\frac{\mathbf{u}}{\|\mathbf{u}\|_\infty}\right) \mathbf{u}_{\max}$.

Fig. 4a shows snapshots of the system trajectories avoiding each obstacle and converging to the target. The trajectories avoid each obstacle \mathbf{X}_{u_k} (labeled 1, ..., 4) at $t = 17$ s, 20 s, 34 s, and 37 s, respectively.

Fig. 4b shows the distance between the system trajectory and obstacles $d_k = \|\mathbf{x} - \mathbf{X}_{u_k}\|$ over time. It can be seen that this distance is always greater than zero for all time, indicating that the system trajectories never enter the unsafe set. The corresponding control inputs are shown in 4c. Note that the control inputs stay within the bounds defined by $\mathbf{u}_{\max} = 2$.

B. Collision Avoidance in Multi-agent Systems

In this section, we demonstrate the application of the proposed density-based controller to a multi-agent collision avoidance problem. Let \mathbf{x}_j for $j = 1, \dots, N$ be the state of the N agents. Let \mathbf{X}_{u_k} be the region around the agent \mathbf{x}_k where no other agent can enter. \mathbf{X}_{u_k} can be the physical space that the agent occupies, in which case \mathbf{x}_k is the center of the \mathbf{X}_{u_k} or a safe bubble around the agent \mathbf{x}_k . We assume this region to be circular as defined in (5). Similarly, we define the sensing region around $\mathbf{X}_{u_k}(t)$ denoted by $\mathbf{X}_{s_k}(t)$ where other agents, $\mathbf{x}_{i \neq k}(t)$ can sense the presence of agent $\mathbf{x}_k(t)$ for $i, k = 1, \dots, N$ using (7).

In the following, we provide the construction of density functions for multi-agent systems. Let $\rho_j(t, \mathbf{x}_j)$ be the density function of j^{th} agent. We have the following construction of the density function.

$$\rho_j(t, \mathbf{x}_j) = \frac{\Phi^j(t, \mathbf{x}_j)}{V_1^j(\mathbf{x}_j)} \quad (20)$$

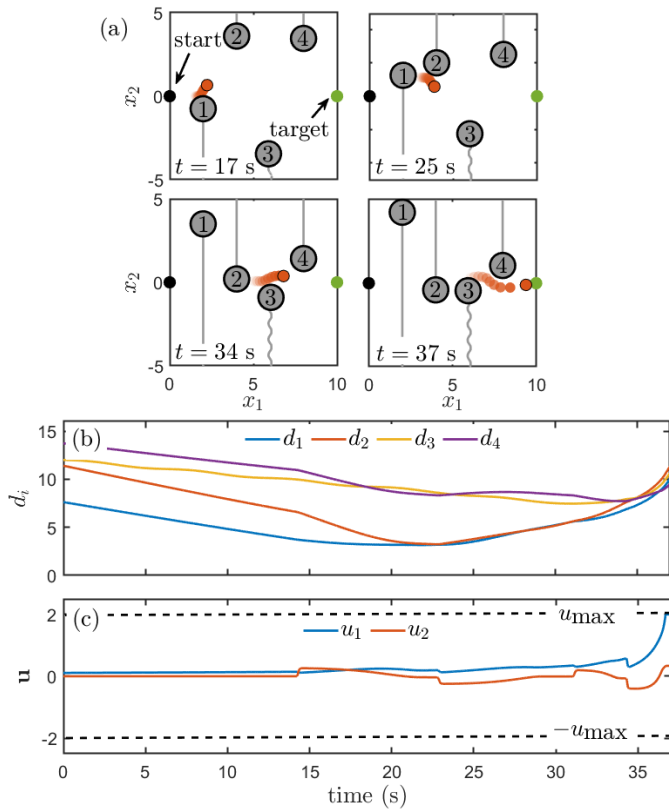


Fig. 4. **Dynamic Unsafe Set:** Snapshots of the system trajectory (red) converging to the target (green) while avoiding time-varying obstacles (gray).

where $\Phi^j(t, \mathbf{x}_j)$ is of the form

$$\Phi^j(t, \mathbf{x}_j) = \prod_{k \neq j}^N \Psi_k^j(t, \mathbf{x}_k) \quad (21)$$

where $\Psi_k^j(t, \mathbf{x}_k)$ is defined as follows

$$\Psi_k^j(t, \mathbf{x}_k) := \begin{cases} \theta, & \mathbf{x}_j \in \mathbf{X}_{u_k}(t) \\ \phi_k(\mathbf{x}_j - \mathbf{x}_k(t)), & \mathbf{x}_j \in \mathbf{X}_{s_k}(t) \\ 1, & \text{otherwise} \end{cases} \quad (22)$$

The function $\phi_k(\mathbf{x}_j - \mathbf{x}_k(t))$ is as defined in (9). The function $V_1^j(\mathbf{x}_j)$ encodes the target information \mathbf{z}_j for the agent \mathbf{x}_j and can be defined as follows

$$V_1^j(\mathbf{x}_j) = \frac{1}{\|\mathbf{x}_j - \mathbf{z}_j\|^{\alpha + \kappa}} \quad (23)$$

for some constant $\kappa > 0$. The function $\phi_k(\mathbf{x}_j - \mathbf{x}_k(t))$ is as defined in (9).

The regions, $\mathbf{X}_{u_k}(t)$ and $\mathbf{X}_{s_k}(t)$ play a role similar to the regions defined in (4) and (6) as the dynamic agent $\mathbf{x}_k(t)$ for acts as a time-varying obstacle to j^{th} agent for $k = 1, \dots, N \neq j$. The dynamics of the j^{th} agent is then given by

$$\dot{\mathbf{x}}_j = \beta \nabla \rho_j(t, \mathbf{x}_j) \quad (24)$$

for $j = 1, \dots, N$.

Remark 8: It is important to emphasize that while the construction of the density function $\rho_j(t, \mathbf{x}_j)$ in Eq. (20) involves the knowledge of all the agents, the construction of function, Ψ_k^j and ϕ_k in Eqs. (21) and (22) is such that the individual agents do not need to know the states of other agents until the sensing regions of the two agents collide. Hence, the collision avoidance dynamics can be executed in a distributed manner without having access to the global information of all the agents.

Next, we set up an example to simulate an intersection where the agents have to avoid collision with each other while reaching their target. Consider six agents whose internal dynamics are given by

$$\dot{x}_j = v_j \cos \delta_j, \quad \dot{y}_j = v_j \sin \delta_j, \quad \dot{\delta}_j = \omega_j$$

for $j = 1, \dots, 6$. Here, the control inputs are v_j and ω_j , which are the linear and angular velocities of agent j , respectively.

We use the integrator dynamics defined in (24) where $\mathbf{x}_j = [x_j, y_j]$ and $\mathbf{u}_j = [u_{j_x}, u_{j_y}]$. The density function for each agent is defined using (11), where every other agent is modeled as a disk. Then, v_j and ω_j can be obtained as follows

$$v_j = \sqrt{u_{j_x}^2 + u_{j_y}^2}, \quad \omega_j = \dot{\delta}_j - K(\delta_j - \tilde{\delta}_j),$$

where $K > 0$ is a positive gain and $\tilde{\delta} = \tan^{-1} \left(\frac{u_{j_y}}{u_{j_x}} \right)$. The control ω is designed such that the error $(\delta - \tilde{\delta})$ tends to zero asymptotically. This can be shown using a Lyapunov function as $V = \frac{1}{2} (\delta - \tilde{\delta})^2$.

Fig. 5 presents snapshots of six agents navigating an intersection and reaching their targets. Each agent is depicted as a solid circle, with a larger, transparent circle representing their sensing region. For clarity, we show the sensing region of each agent only in the first timestamp. Each agent's start and target positions are marked by a solid point and a hollow circle (with corresponding colors), respectively. The trajectories are shown as dashed lines, and the heading angles are indicated by solid lines extending from the agents.

In scenario 1 (top row), all agents are modeled as disks with a radius $r_j = 0.5$ and a circular sensing radius of $s_j = 2$. Around $t = 3$ s, agents 5 and 6 resolve a conflict by executing circular maneuvers. The other agents initially slow down and resolve their conflict by performing circular maneuvers around $t = 7$ s before converging on their targets after $t = 9$ s. In scenario 2 (bottom row), agents 5 and 6 have a radius of $r_5 = 1$ and $r_6 = 1$, respectively. The corresponding sensing radius is set to $s_5 = 3$ and $s_6 = 3$, respectively. Agents 1 and 2 slow down initially and resolve conflicts around $t = 7$ s. The larger agents (agents 5 and 6) push the smaller agents (agents 2 and 4) away from their shortest path trajectory (see timestamp $t = 4$ s) before converging to the target. Eventually, agents 2 and 3 perform a course correction maneuver around $t = 7$ s and resolve their conflicts around $t = 10$ s before converging to their respective targets.

Remark 9: Since the convergence of each agent is with respect to almost everywhere sense, as defined by Definition 2, there is still a possibility of gridlock. This arises when the initial condition of agent j lies in its zero-measure set.

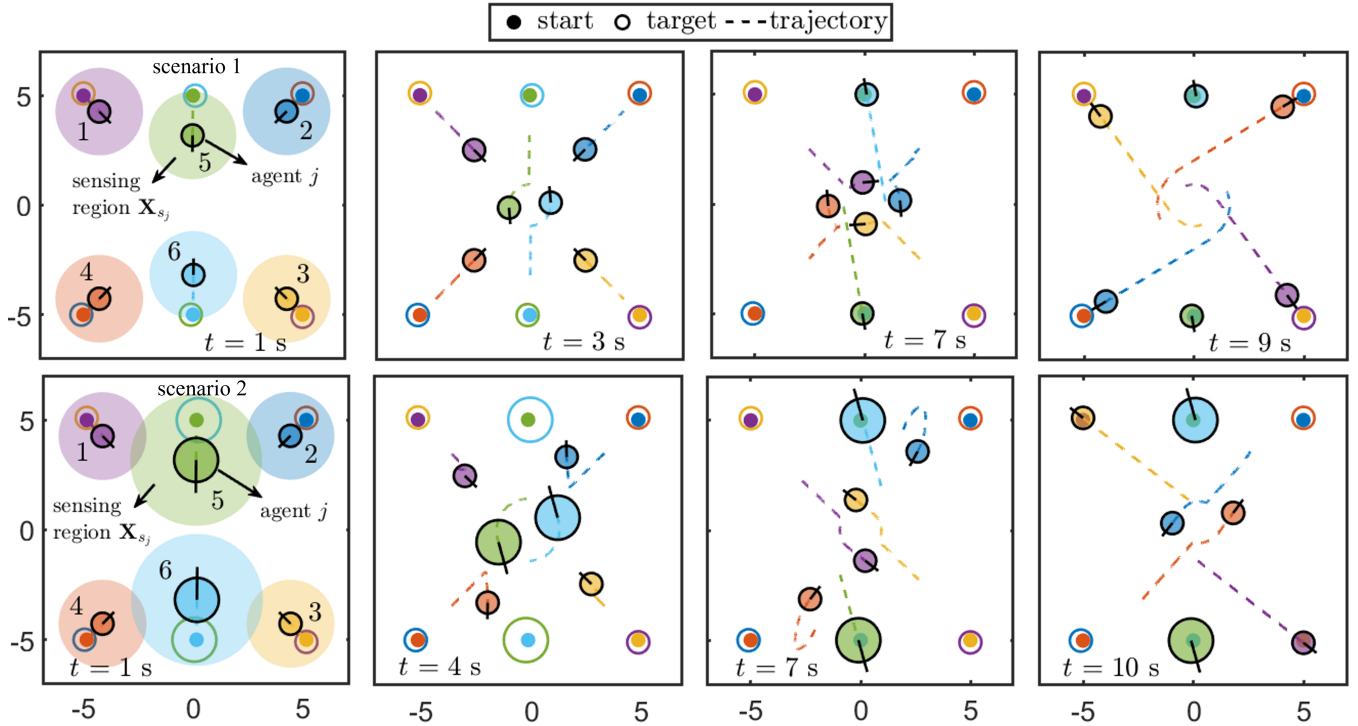


Fig. 5. **Multi-agent Collision Avoidance:** Snapshots of interactions between six agents navigating an intersection while avoiding gridlock. Scenario 1 (top row) shows six identical agents, and Scenario 2 (bottom row) shows agents 5 and 6 having twice the radius as the other agents.

Obtaining theoretical guarantees for avoiding gridlock is left for future work.

1) *Comparison with Social Force Model:* This section compares the simulation results for multi-agent collision avoidance obtained using our proposed approach with the social force model (SFM), which is a popular model for simulating collective human behavior [12].

For this comparison, we set up a scenario with four agents where each agent has to swap positions with the opposite agent. The agents are modeled as a disk of radius $r_j = 0.75$ using double integrator dynamic given by

$$\dot{\mathbf{x}}_j = \mathbf{v}_j, \quad \dot{\mathbf{v}}_j = \mathbf{u}_j.$$

where $\mathbf{x}_j \in \mathbb{R}^2$ and $\mathbf{v}_j \in \mathbb{R}^2$. First, we use the SFM to define the control for this system. This force-based method is used to represent human motion as a sum of desired forces, f_{d_j} and repulsive forces, f_{r_j} (as described in [13]).

$$\mathbf{u}_j = \mathbf{u}_j^{SFM} := f_{d_j} + f_{r_j} \quad (25)$$

Next, we design a density-based controller for double integrator dynamics as follows

$$\mathbf{u}_j^p(t, \mathbf{x}_j) = \frac{d}{dt} (\beta \nabla \rho_j(t, \mathbf{x}_j)) - K (\mathbf{v}_j - \beta \nabla \rho_j(t, \mathbf{x}_j)) \quad (26)$$

where $K > 0$. The stability of this controller can be verified using the Lyapunov function $V = \frac{1}{2} (\mathbf{v}_j - \beta \nabla \rho(t, \mathbf{x}_j))^2$.

Fig. 6 shows snapshots of the interaction between the four agents (with unit mass and radius of 0.75) as they avoid conflict and converge to the target. In the top row, each agent

uses the density-based controller \mathbf{u}_j^p . We construct the density function $\rho_j(t, \mathbf{x}_j)$ as defined in (20). For each agent, we use $r_j = 0.75$, $s_j = 2$ in the construction of $\Phi_j(t, \mathbf{x}_j)$ and define $V_1^j = \|\mathbf{x}_j - \mathbf{z}_j\|^2$. Further, we use $\alpha = 0.2$ and $\beta = 20$, $K = 1$. The agents approach the conflict region at around $t = 3$ s and execute a circular maneuver to resolve the conflict at $t = 4.5$ s before converging to the target at $t = 5.5$ s. The bottom row shows the multi-agent interaction when each agent executes the SFM-based controller \mathbf{u}_j^{SFM} . We model each agent as identical circular disks with $r_j = 0.75$, $r_k = 0.75$, and a sensing distance of $d_H = 2$. Further, we use $A_j = 2000$, $B_j = 0.08$, $\kappa_1 = 1.2 \times 10^5$ and $\kappa_2 = 2.4 \times 10^5$.

While resolving conflicts, the SFM-based controller leads to oscillations (see timestamp $t = 2.5$ s, bottom row) since the agents behave like particles, while the density-based controller results in smooth trajectories (see timestamp $t = 4.5$ s, top row). Further, to the best of our knowledge, the SFM model does not provide any theoretical guarantees for ensuring safety and convergence.

C. Robotic Arm Trajectory Tracking

In this section, we extend the density-based controller proposed in Theorem 2 to fully actuated robotic systems whose dynamics can be expressed using the Euler-Lagrange equations. Consider an unconstrained system with \mathbf{q} and $\dot{\mathbf{q}}$ being the position and velocity states respectively. Let \mathbf{Q} be the configuration manifold of the robot and $\mathbf{q} \in \mathbf{Q}$. For a two-link planar robotic arm, $\mathbf{q} \in \mathbf{S}^1 \times \mathbf{S}^1$ represents the angle position

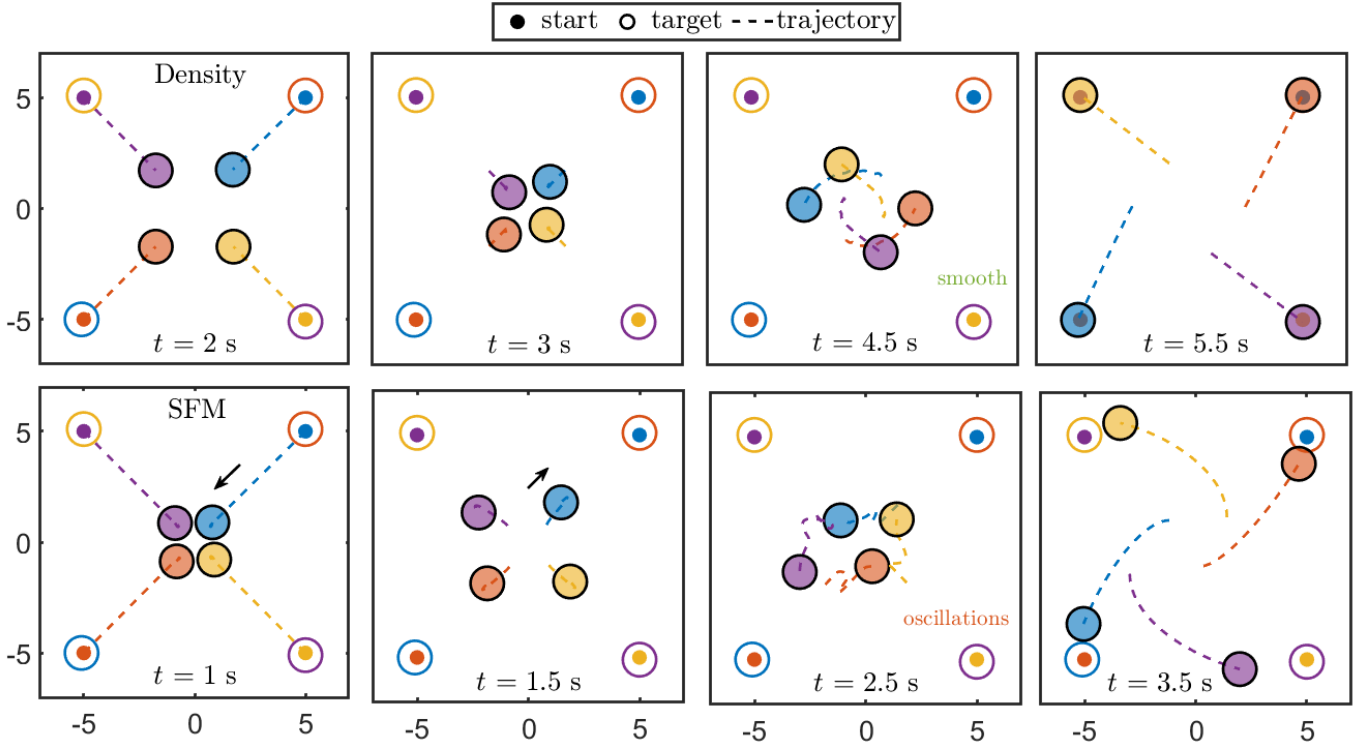


Fig. 6. **Comparison with social force model:** The agents using the density-based controller resolve conflicts and converge to the target smoothly (top row), while the SFM-based controller can lead to oscillations (bottom row).

of each link. Let $\mathbf{M}(\mathbf{q})$ be the inertia matrix and $\mathbf{H}(\mathbf{q}, \dot{\mathbf{q}})$ represent the Coriolis and gravity effects on the system. The dynamics of the system can be defined as follows

$$\mathbf{M}(\mathbf{q})\ddot{\mathbf{q}} + \mathbf{H}(\mathbf{q}, \dot{\mathbf{q}}) = \mathbf{u}_\rho(t, \mathbf{q}, \dot{\mathbf{q}}) \quad (27)$$

The typical approach involves a hierarchical structure that separates navigation into two stages: motion planning and control. In motion planning, the task is to determine a collision-free path or trajectory through the feasible configuration space, starting from an initial state and ending at a desired goal. This trajectory serves as the input for the control stage, where several existing methods, such as model predictive control, can be used to design appropriate control actions to follow the planned path, ensuring dynamic feasibility.

In the following, we outline how the proposed density-based approach can be used as a motion plan for such systems. We first construct a time-varying density function in the configuration space ρ_q as follows

$$\rho_q(t, \mathbf{q}) = \frac{\prod_{k=1}^L \Psi(\mathbf{q})}{(V_q(t, \mathbf{q}))^\alpha} \quad (28)$$

$$\rho_{0_q}(t, \mathbf{q}) = \frac{\prod_{k=1}^L \Psi(\mathbf{q})}{(V_q(t, \mathbf{q}) + \kappa)^\alpha} \quad (29)$$

where $V_q(t, \mathbf{q})$ is a distance function that encodes the target trajectory (defined based on the underlying configuration space), $\Psi_k(\mathbf{q})$ are inverse bump functions used to represent the obstacles in the configuration space. Next, we generate a safe path that avoids static obstacles while tracking a time-varying

target as a solution to the following system

$$\dot{\mathbf{q}} = \nabla \rho_{0_q}(t, \mathbf{q}) \quad (30)$$

The solution $\mathbf{q}(t)$ can serve as the safe motion plan in designing safe navigation frameworks. This approach has been successfully employed for the safe navigation of quadruped robots and ground vehicles in [34], [38], [39].

Next, we use a two-link robotic arm to track a time-varying target while avoiding static unsafe sets. The system's dynamics can be given by (27). The mass and length of each link are set to unity. We assume that the system is fully actuated (i.e., there is a torque input at both joints), and the obstacles are present only in the position states.

To construct the density functions, the task space obstacles (circular with a radius of 0.2) are mapped to configuration space and approximated using inverse bump functions. Further, we use the following storage function

$$V_q(t, \mathbf{q}) = \left(1 - \cos(\bar{q}_1)\right)^2 + \left(1 - \cos(\bar{q}_2)\right)^2,$$

where $\bar{q}_i = q_i - q_{i_T}(t)$, and construct the density function using (28). Here $[q_{1_T}(t), q_{2_T}(t)]$ represents the target trajectory. The objective is to track the trajectory of a time-varying target (in task space) given by $\mathbf{x}_T(t) = [0.5 + \sin(t), -0.6 - \cos(t)]$.

First, a safe path for this system should be designed that avoids all the unsafe sets while tracking a time-varying target. Specifically, the motion plan is obtained as a solution to the system $\dot{\mathbf{q}} = \beta \nabla \rho_{0_q}(t, \hat{\mathbf{q}})$. Next, we define a density-based

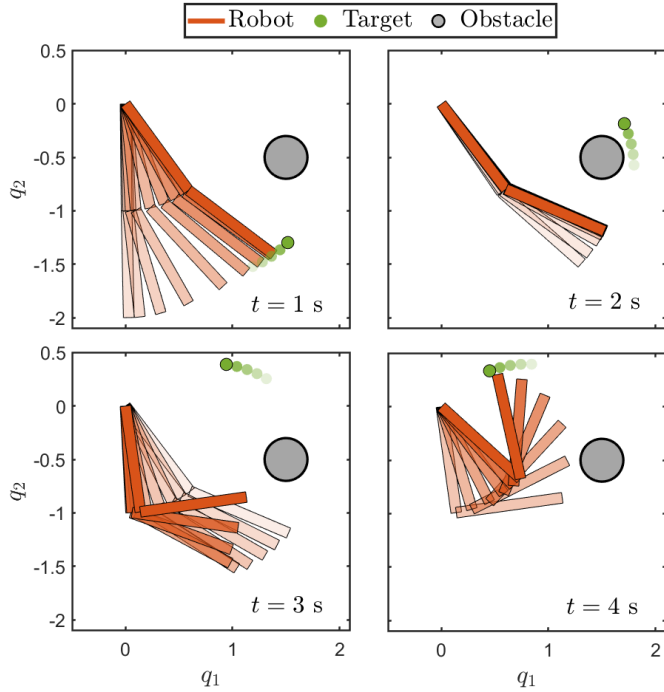


Fig. 7. **Robotic Arm Trajectory Tracking with safety:** Snapshots of the robot (red) tracking a time-varying target $\mathbf{x}_T(t)$ (green) while avoiding the unsafe set \mathbf{X}_u .

inverse dynamics controller given by

$$\mathbf{u}_\rho = \mathbf{M}(\mathbf{q}) \left(\ddot{\mathbf{q}}_d(t) - \mathbf{K}_p \mathbf{e}(t) - \mathbf{K}_v \dot{\mathbf{e}}(t) \right) + \mathbf{H}(\mathbf{q}, \dot{\mathbf{q}}) \quad (31)$$

where $\mathbf{e}(t) := \mathbf{q}(t) - \mathbf{q}_d(t)$ and $\dot{\mathbf{e}}(t) := \dot{\mathbf{q}}(t) - \dot{\mathbf{q}}_d(t)$, $\mathbf{q}_d(t)$ is the desired reference trajectory which is obtained from the motion plan. \mathbf{K}_p and \mathbf{K}_v are constant gain matrices.

Using the controller defined in (31), the system dynamics defined in (27) reduces to

$$\ddot{\mathbf{e}} + \mathbf{K}_v \dot{\mathbf{e}} + \mathbf{K}_p \mathbf{e} = 0. \quad (32)$$

Hence, by choosing $\mathbf{K}_p > 0$ and $\mathbf{K}_v > 0$, it can be easily verified that the above system is asymptotically stable, i.e., the tracking errors \mathbf{e} and $\dot{\mathbf{e}}$ go to zero asymptotically.

Remark 10: Note that the system's safety is not guaranteed if the system is only asymptotically stable. However, with large enough gains and a suitable Lyapunov function, it can be shown that the system is exponentially stable, i.e., the error goes to zero in a finite time.

Fig. 7 shows snapshots of the system tracking a circular target trajectory while avoiding obstacles. We use $\beta = 10$ to obtain the motion plan and set $\mathbf{K}_p = 1$ and $\mathbf{K}_v = 10$ for the inverse dynamics controller. The system starts tracking the target at $t = 1$ s while avoiding the obstacle between $t = 2$ s and $t = 3$ s before converging to the target again at $t = 4$ s.

V. CONCLUSIONS

This paper presented a novel approach to addressing the challenges of safe navigation in dynamic environments. We

introduced an analytical method for constructing density functions for two key scenarios: time-varying obstacles with static targets and time-varying target trajectories with static obstacles. Central to our approach is the development of a density-based feedback controller that guarantees safety while ensuring almost everywhere convergence in both cases. The proposed framework was further validated through its application to multi-agent systems and robotics, demonstrating its effectiveness in collision avoidance and safe trajectory tracking for robotic arms. These results underscore the practical utility of our method in real-world robotic control scenarios, particularly in environments requiring dynamic adaptability.

VI. APPENDIX

The proof of Theorem 1 is presented in this Appendix. This proof relies on Theorem 2.2 from [40] and Proposition 2.1 from [41], which are stated below as Lemma 1 and Theorem 3 respectively for the sake of completeness.

Lemma 1 ([40] Theorem 2.2): Given time-varying system dynamics $\dot{\mathbf{x}}(t) = \mathbf{f}(t, \mathbf{x})$, if there exists a non-negative integrable function $\rho(t, \mathbf{x}) \in \mathcal{C}^1(\mathbb{R} \times \mathbf{X}_1, \mathbb{R})$ such that

$$\frac{\partial \rho}{\partial t} + \nabla \cdot (\mathbf{f}(t, \mathbf{x}) \rho(t, \mathbf{x})) > 0, \quad \text{a.e. } (t, \mathbf{x}) \in \mathbb{R} \times \mathbf{X}_1, \quad (33a)$$

$$\int_{\mathbb{R} \times \mathbf{X}_1} \frac{1 + \|\mathbf{f}(t, \mathbf{x})\|}{1 + \|\mathbf{x}\|} \rho(t, \mathbf{x}) dx dt < \infty \quad (33b)$$

then the system trajectories will converge to \mathbf{X}_T for almost all initial condition (w.r.t. Lebesgue measure) inside \mathbf{X}_1 .

The results of Theorem 1 provide the condition of a.e. convergence of time-varying systems and can be viewed as an extension of results from [42] to time-varying setting. We state the results from [41][Proposition 2.1] for the purpose of completion.

Theorem 3 ([41] Proposition 2.1): Consider the time-varying system dynamics $\dot{\mathbf{x}}(t) = \mathbf{f}(t, \mathbf{x})$, and a non-negative integrable function $\rho(t, \mathbf{x}) \in \mathcal{C}^1(\mathbb{R} \times \mathbf{X}_1, \mathbb{R})$. Let $s_t(t_0, \mathbf{x})$ be the solution of the system $\dot{\mathbf{x}} = \mathbf{f}(t, \mathbf{x})$. If $Z \subset \mathbf{X}_1$ be a Borelian set, then for all $t_0 \leq \tau \leq t$, we can show that

$$\int_{s_t(t_0, \mathbf{Z})} \rho(t, \mathbf{x}) dx - \int_{\mathbf{Z}} \rho(t_0, \mathbf{x}) dx = \int_{t_0}^t \int_{s_\tau(t_0, \mathbf{Z})} \left[\frac{\partial \rho(\tau, \mathbf{x})}{\partial \tau} + \nabla \cdot (\mathbf{f} \rho) \right](\tau, \mathbf{x}) dx d\tau \quad (34)$$

The results of Theorem 3 can be viewed as an extension of classical Liouville results for an autonomous system with a time-invariant density function [43].

Proof: [Proof of Theorem 1]

We will first utilize Lemma 1 to show that the dynamical system given in (13) will converge to the target set \mathbf{X}_T in an almost everywhere sense by finding the appropriate range of α and β .

Convergence: We consider the closed loop dynamics given by (13) and the density function given by

$$\rho(t, \mathbf{x}) = \frac{\Psi(t, \mathbf{x})}{V(\mathbf{x})^\alpha} \quad (35)$$

To show that the trajectories of this system converge to the target \mathbf{X}_T from almost all initial conditions, we will utilize Lemma 1 and prove that the following inequality is satisfied.

$$\nabla \cdot (\mathbf{k}(t, \mathbf{x})\rho(t, \mathbf{x})) + \frac{\partial \rho}{\partial t} > 0, \quad a.e. (t, \mathbf{x}) \in \mathbb{R} \times \mathbf{X}_1, \quad (36a)$$

$$\int_{\mathbb{R} \times \mathbf{X}_1} \frac{1 + \|\mathbf{k}(t, \mathbf{x})\|}{1 + \|\mathbf{x}\|} \rho(t, \mathbf{x}) dx dt < \infty \quad (36b)$$

Validity of (36a): We will show that each term on the left-hand side of (36a) is greater than zero. We will first expand the divergence term, $\nabla \cdot (\mathbf{k}\rho)$, and find the range of α for which this term is greater than zero. Similarly, we will find the range of β for which the time derivative term, $\frac{\partial \rho}{\partial t}$, is greater than zero. The steps are given below.

Range of α : We will find the range of α by expanding the divergence term given by

$$\nabla \cdot (\mathbf{k}(t, \mathbf{x})\rho(t, \mathbf{x})) = \beta \left(\rho(t, \mathbf{x}) \sum_{j=1}^n \frac{\partial^2 \rho_o}{\partial x_j^2} + \frac{\partial \rho_o}{\partial \mathbf{x}} \frac{\partial \rho}{\partial \mathbf{x}}^\top \right). \quad (37)$$

Now we know that $\rho(t, \mathbf{x}) > 0$. Also,

$$\begin{aligned} \frac{\partial \rho_o}{\partial \mathbf{x}} \frac{\partial \rho}{\partial \mathbf{x}}^\top &= \sum_{j=1}^n \frac{\partial \rho_o}{\partial x_j} \frac{\partial \rho}{\partial x_j} \\ &= \sum_{j=1}^n \left(\frac{\alpha^2}{V^{\alpha+1} V_1^{\alpha+1}} \Psi^2 \left[\frac{\partial V}{\partial x_j} \right]^2 \right) \\ &\quad + \left(\frac{1}{V^\alpha V_1^\alpha} \left[\frac{\partial \Psi}{\partial x_j} \right]^2 \right) - \left(\frac{\alpha}{V^\alpha V_1^{\alpha+1}} \Psi \frac{\partial V}{\partial x_j} \frac{\partial \Psi}{\partial x_j} \right) \\ &\quad - \left(\frac{\alpha}{V^{\alpha+1} V_1^\alpha} \Psi \frac{\partial V}{\partial x_j} \frac{\partial \Psi}{\partial x_j} \right) \end{aligned} \quad (38)$$

and

$$\begin{aligned} \rho \frac{\partial^2 \rho_o}{\partial x_j^2} &= \frac{\alpha \Psi}{V^\alpha V_1^\alpha} \left[\frac{\alpha+1}{V_1^2} \Psi \left(\frac{\partial V}{\partial x_j} \right)^2 - \frac{1}{V_1} \Psi \frac{\partial^2 V}{\partial x_j^2} \right. \\ &\quad \left. - \frac{2}{V_1} \frac{\partial \Psi}{\partial x_j} \frac{\partial V}{\partial x_j} + \frac{\partial^2 \Psi}{\partial x_j^2} \frac{1}{\alpha} \right] \end{aligned} \quad (39)$$

Therefore, using (38) and (39), we can write (37) as follows:

$$\begin{aligned} \nabla \cdot (\mathbf{k}\rho) &= \frac{\alpha\beta}{V^\alpha V_1^\alpha} \sum_{j=1}^n \left[\left(\frac{\alpha}{V V_1} + \frac{\alpha+1}{V_1^2} \right) \Psi^2 \left(\frac{\partial V}{\partial x_j} \right)^2 \right. \\ &\quad - \left(\frac{3}{V_1} + \frac{1}{V} \right) \Psi \frac{\partial V}{\partial x_j} \frac{\partial \Psi}{\partial x_j} - \frac{\Psi^2}{V_1} \frac{\partial^2 V}{\partial x_j^2} \\ &\quad \left. + \frac{1}{\alpha} \left(\Psi \frac{\partial^2 \Psi}{\partial x_j^2} + \left(\frac{\partial \Psi}{\partial x_j} \right)^2 \right) \right] \end{aligned} \quad (40)$$

Therefore, when $\mathbf{x} \in \mathbf{X}_{s_k}$, using Assumption 2.4 and 2.5, we get the following bounds.

$$\begin{aligned} \left(\frac{\alpha}{V V_1} + \frac{\alpha+1}{V_1^2} \right) \Psi^2 \left(\frac{\partial V}{\partial x_j} \right)^2 &\geq \\ (2\alpha+1)(\bar{d}_V \|\mathbf{x}\|^2 + \kappa)^{-2} \theta^2 (\underline{d}_{V_x})^2 \|\mathbf{x}\|^2 \end{aligned} \quad (41)$$

$$\left(\frac{3}{V_1} + \frac{1}{V} \right) \Psi \frac{\partial V}{\partial x_j} \frac{\partial \Psi}{\partial x_j} \leq 4(\underline{d}_V)^{-1} \bar{d}_{V_x} \bar{c}_{\Psi_x} \|\mathbf{x}\|^{-1} \quad (42)$$

$$\frac{\Psi^2}{V_1} \frac{\partial^2 V}{\partial x_j^2} \leq \kappa^{-1} \bar{d}_{V_{x_2}} \quad (43)$$

$$\frac{1}{\alpha} \left(\Psi \frac{\partial^2 \Psi}{\partial x_j^2} + \left(\frac{\partial \Psi}{\partial x_j} \right)^2 \right) \geq \frac{-1}{\alpha} (\bar{c}_{\Psi_{x_2}}) \quad (44)$$

Now, using Assumption 2.2, we can assume that $\underline{c}_x \leq \|\mathbf{x}\| \leq \bar{c}_x$ for some $\underline{c}_x, \bar{c}_x > 0$. Therefore, we can rewrite (41)-(42) as follows:

$$\begin{aligned} \left(\frac{\alpha}{V V_1} + \frac{\alpha+1}{V_1^2} \right) \Psi^2 \left(\frac{\partial V}{\partial x_j} \right)^2 &\geq \\ (2\alpha+1)(\bar{d}_V (\bar{c}_x)^2 + \kappa)^{-2} \theta^2 (\underline{d}_{V_x})^2 (\bar{c}_x)^2 \end{aligned} \quad (45)$$

$$\left(\frac{3}{V_1} + \frac{1}{V} \right) \Psi \frac{\partial V}{\partial x_j} \frac{\partial \Psi}{\partial x_j} \leq 4(\underline{d}_V)^{-1} \bar{d}_{V_x} \bar{c}_{\Psi_x} (\underline{c}_x)^{-1} \quad (46)$$

Therefore, utilizing (43)-(46), we get the following lower bound for all $\mathbf{x} \in \mathbf{X}_{s_k}$

$$\begin{aligned} \nabla \cdot (\mathbf{k}\rho) &\geq \frac{\alpha\beta n}{V^\alpha V_1^\alpha} \left((2\alpha+1)(\bar{d}_V (\bar{c}_x)^2 + \kappa)^{-2} \theta^2 (\underline{d}_{V_x})^2 (\bar{c}_x)^2 \right. \\ &\quad \left. - 4(\underline{d}_V)^{-1} \bar{d}_{V_x} \bar{c}_{\Psi_x} (\underline{c}_x)^{-1} - \kappa^{-1} \bar{d}_{V_{x_2}} - \frac{1}{\alpha} (\bar{c}_{\Psi_{x_2}}) \right) \end{aligned} \quad (47)$$

Similarly, when $\mathbf{x} \notin \mathbf{X}_{s_k}$, using Assumption 2.4 and 2.5, and the fact that both $\frac{\partial \Psi}{\partial x_j} = 0$ and $\frac{\partial^2 \Psi}{\partial x_j^2} = 0$, we get the following bounds.

$$\begin{aligned} \nabla \cdot (\mathbf{k}\rho) &\geq \frac{\alpha\beta n}{V^\alpha V_1^\alpha} \left((2\alpha+1)(\bar{d}_V \|\mathbf{x}\|^2 + \kappa)^{-2} \right. \\ &\quad \left. \theta^2 (\underline{d}_{V_x})^2 \|\mathbf{x}\|^2 - (\underline{d}_V)^{-1} \bar{d}_{V_{x_2}} \|\mathbf{x}\|^{-2} \right) \end{aligned} \quad (48)$$

As $\mathbf{x} \in \mathbf{X}_1 : \mathbf{X} \setminus B_\delta$, we have

$$\bar{d}_V \|\mathbf{x}\|^2 + \kappa \leq \bar{d}_{V_1} \|\mathbf{x}\|^2 \quad (49)$$

where we choose

$$\bar{d}_{V_1} \geq \bar{d}_V + \frac{\kappa}{\delta} \quad (50)$$

Therefore, using (49), we can rewrite (48) as follows:

$$\begin{aligned} \nabla \cdot (\mathbf{k}\rho) &\geq \frac{\alpha\beta n \|\mathbf{x}\|^{-2}}{V^\alpha V_1^\alpha} \left((2\alpha+1)(\bar{d}_{V_1})^{-2} \theta^2 (\underline{d}_{V_x})^2 \right. \\ &\quad \left. - (\underline{d}_V)^{-1} \bar{d}_{V_{x_2}} \right) \end{aligned} \quad (51)$$

Next, we will show that for any $\theta > 0$, there exists a value of α for which the lower bounds in (47) and (51) are positive. To ensure that the lower bound in (51) is positive, we require that

$$\alpha > \frac{0.5(\underline{d}_V)^{-1} \bar{d}_{V_{x_2}}}{(\bar{d}_{V_1})^{-2} \theta^2 (\underline{d}_{V_x})^2} - 0.5 \quad (52)$$

Next, we can write the right hand side of (47) compactly as follows:

$$\frac{\beta n}{V^\alpha V_1^\alpha} (p_1 \alpha^2 + p_2 \alpha + p_3)$$

where,

$$\begin{aligned} p_1 &= 2((\bar{d}_V)^{-1}(\bar{c}_x)^{-2} + \kappa)^{-2}\theta^2(\underline{d}_{V_x})^2(\bar{c}_x)^2\theta \\ p_2 &= ((\bar{d}_V)^{-1}(\bar{c}_x)^{-2} + \kappa)^{-2}\theta^2(\underline{d}_{V_x})^2(\bar{c}_x)^2\theta \\ &\quad - 4(\underline{d}_V)^{-1}\bar{d}_{V_x}\bar{c}_{\Psi_x}(\bar{c}_x)^{-1} - \kappa^{-1}\bar{d}_{V_{x_2}} \\ p_3 &= -\bar{c}_{\Psi_{x_2}} \end{aligned}$$

We observe that for $\theta > 0$, the term inside the brackets in (47) is a convex quadratic function since its Hessian is given by $2p_1 > 0$. Also, we infer that one of the roots of this quadratic function is positive since $p_2^2 - 4p_1p_3 > 0$. Therefore the range of α which makes the lower bound in (47) positive is given by

$$\alpha > \frac{-p_2 + \sqrt{p_2^2 - 4p_1p_3}}{2p_1} > 0 \quad (53)$$

Therefore, from (52) and (53), we obtain the following condition on the choice of α to make the lower bounds in (51) and (47) positive.

$$\alpha > \max \left\{ \frac{0.5(\underline{d}_V)^{-1}\bar{d}_{V_{x_2}}}{(\bar{d}_{V_1})^{-2}\theta^2(\underline{d}_{V_x})^2} - 0.5, \frac{-p_2 + \sqrt{p_2^2 - 4p_1p_3}}{2p_1} \right\} \quad (54)$$

In summary, using the above choice of α , we have

$$\begin{aligned} \nabla \cdot (\mathbf{k}\rho) &\geq \frac{\alpha\beta n \|\mathbf{x}\|^{-2}}{V^\alpha V_1^\alpha} ((2\alpha + 1)(\bar{d}_{V_1})^{-2}\theta^2(\underline{d}_{V_x})^2 \\ &\quad - (\underline{d}_V)^{-1}\bar{d}_{V_{x_2}}) > 0 \quad \forall \mathbf{x} \notin \mathbf{X}_{s_k} \end{aligned} \quad (55)$$

$$\begin{aligned} \nabla \cdot (\mathbf{k}\rho) &\geq \frac{\alpha\beta n}{V^\alpha V_1^\alpha} ((2\alpha + 1)(\bar{d}_V(\bar{c}_x)^2 + \kappa)^{-2}\theta^2(\underline{d}_{V_x})^2(\bar{c}_x)^2) \\ &\quad - \frac{\alpha\beta n}{V^\alpha V_1^\alpha} (4(\underline{d}_V)^{-1}\bar{d}_{V_x}\bar{c}_{\Psi_x}(\bar{c}_x)^{-1} + \kappa^{-1}\bar{d}_{V_{x_2}}) \\ &\quad - \frac{\alpha\beta n}{V^\alpha V_1^\alpha} \left(\frac{1}{\alpha} (\bar{c}_{\Psi_{x_2}}) \right) > 0 \quad \forall \mathbf{x} \in \mathbf{X}_{s_k} \end{aligned} \quad (56)$$

Range of β : Next, we will select the positive constant β such that the time derivative term, $\frac{\partial \rho}{\partial t}$, in (36a) is greater than zero. When $\mathbf{x} \notin \mathbf{X}_{s_k}$, from the construction of ρ as given in (10) and (35), we conclude that

$$\frac{\partial \rho}{\partial t} = 0 \implies (36a) > 0, \quad \forall \beta > 0$$

Next, when $\mathbf{x} \in \mathbf{X}_{s_k}$, utilizing Assumption 2.4, we have

$$\begin{aligned} \left| \frac{\partial \rho_o}{\partial t} \right| &= \frac{1}{V_1^\alpha} \left| \frac{\partial \Psi}{\partial t} \right| \\ \left| \frac{\partial \rho_o}{\partial t} \right| &\leq \frac{1}{V_1^\alpha} c_{\psi_t} \end{aligned} \quad (57)$$

Similarly, rewriting (56), we get

$$\nabla \cdot (\mathbf{k}(\mathbf{x}, t)\rho) \geq \frac{\beta L_1}{V_1^\alpha} > 0 \quad (58)$$

where L_1 is obtained from the right hand side of (56) and given by

$$\begin{aligned} L_1 &= \alpha n (\bar{d}_V)^{-1}(\bar{c}_x)^{-2} ((2\alpha + 1)(\bar{d}_V(\bar{c}_x)^2 + \kappa)^{-2}\theta^2 \underline{d}_{V_x}^2 \bar{c}_x^2) \\ &\quad - \alpha n (\bar{d}_V)^{-1}(\bar{c}_x)^{-2} (4(\underline{d}_V)^{-1}\bar{d}_{V_x}\bar{c}_{\Psi_x}(\bar{c}_x)^{-1} + \kappa^{-1}\bar{d}_{V_{x_2}}) \\ &\quad - \alpha n (\bar{d}_V)^{-1}(\bar{c}_x)^{-2} \left(\frac{1}{\alpha} (\bar{c}_{\Psi_{x_2}}) \right) \end{aligned}$$

Therefore, the lower bound on β such that (36a) is satisfied for *a.e.* $(t, \mathbf{x}) \in \mathbb{R} \times \mathbf{X}_1$ can be calculated utilizing (57) and (58) as:

$$\frac{1}{V_1^\alpha} (-c_{\Psi_t} + \beta L_1) > 0$$

Therefore,

$$\beta > \frac{c_{\Psi_t}}{L_1} \quad (59)$$

Validity of (36b): Based on Assumptions 2.4 and 2.5, for all $\mathbf{x} \in \mathbf{X}_1$, we can have the following bounds on $k_j(t, \mathbf{x})$ for $j = 1, \dots, n$.

$$\begin{aligned} -\beta \alpha (\kappa)^{-(\alpha+1)} \bar{d}_{V_x} \|\mathbf{x}\| &\leq k_j(t, \mathbf{x}) \leq \\ \beta \alpha (\kappa)^{-(\alpha+1)} \bar{d}_{V_x} \|\mathbf{x}\| &\forall \mathbf{x} \notin \mathbf{X}_{s_k} \end{aligned} \quad (60a)$$

$$\begin{aligned} -\beta \left((\kappa)^{-(\alpha+1)} \bar{d}_{V_x} \|\mathbf{x}\| + (\kappa)^{-\alpha} \bar{c}_{\Psi_x} \right) &\leq k_j(t, \mathbf{x}) \leq \\ \beta \left((\kappa)^{-(\alpha+1)} \bar{d}_{V_x} \|\mathbf{x}\| + (\kappa)^{-\alpha} \bar{c}_{\Psi_x} \right) &\forall \mathbf{x} \in \mathbf{X}_{s_k} \end{aligned} \quad (60b)$$

We know that $\|\mathbf{x}\| \leq \bar{c}_x$ for all $\mathbf{x} \in \mathbf{X}_{s_k}$. Therefore, using this fact and by using the bounds in (60b), we can infer that (36b) is satisfied when $\mathbf{x} \in \mathbf{X}_{s_k}$.

Using (60a), we get the bounds on $\|\mathbf{k}(t, \mathbf{x})\|$ when $\mathbf{x} \notin \mathbf{X}_{s_k}$ as follows:

$$\|\mathbf{k}(t, \mathbf{x})\| \leq \sqrt{n} \alpha \beta (\kappa)^{-(\alpha+1)} \bar{d}_{V_x} \|\mathbf{x}\|$$

Also, when $\mathbf{x} \notin \mathbf{X}_{s_k}$, $\rho(t, \mathbf{x}) = V(\mathbf{x})^{-\alpha}$ and $V(\mathbf{x}) \leq \bar{d}_V \|\mathbf{x}\|^2$. Therefore,

$$\frac{1 + \|\mathbf{k}(t, \mathbf{x})\|}{1 + \|\mathbf{x}\|} \rho(t, \mathbf{x}) \leq \frac{\sqrt{n} \alpha \beta (\kappa)^{-(\alpha+1)} \bar{d}_{V_x} \|\mathbf{x}\|}{(1 + \|\mathbf{x}\|)(\bar{d}_V \|\mathbf{x}\|^2)^\alpha} \quad (61)$$

We observe that when $\mathbf{x} \notin \mathbf{X}_{s_k}$, as $\|\mathbf{x}\| \rightarrow \infty$, the numerator in (61) goes to infinity linearly whereas denominator goes to infinity at a rate of $(2\alpha + 1)$. Therefore, we can conclude that (61) $< \infty$ for all $\mathbf{x} \notin \mathbf{X}_{s_k}$ and hence (36b) is satisfied. This concludes the convergence proof.

Next, We will first utilize Theorem 3 to show that the dynamical system given in (13) will avoid the unsafe set \mathbf{X}_u for some $\theta > 0$.

Avoidance: In the second part of the proof, we show that the system trajectories with respect to $\mathbf{k}(t, \mathbf{x})$ obtained from (13) avoids the unsafe set \mathbf{X}_u . For the system $\dot{\mathbf{x}} = \mathbf{k}(t, \mathbf{x})$, utilizing Theorem 3, we can write the evolution of the densities of the states along system trajectories as follows:

$$\begin{aligned} \int_{s_t(t_0, \mathbf{Z})} \rho(t, \mathbf{x}) d\mathbf{x} - \int_{\mathbf{Z}} \rho(t_0, \mathbf{x}) d\mathbf{x} = \\ \int_{t_0}^t \int_{s_\tau(t_0, \mathbf{Z})} \left[\frac{\partial \rho(\tau, \mathbf{x})}{\partial \tau} + [\nabla \cdot (\mathbf{k}\rho)](\tau, \mathbf{x}) \right] d\mathbf{x} d\tau > 0 \end{aligned} \quad (62)$$

This proof is done through the method of contradiction. First, we notice that the above quantity is greater than zero, following the previous convergence proof, where we showed that (36a) is positive. For a given $t_0 \geq 0$, let there exists an initial condition $\mathbf{x}_0 \in \mathbf{X}_0$ such that $s_T(t_0, \mathbf{x}_0) \in \mathbf{X}_u$ for some $T > t_0$ and $s_t(t_0, \mathbf{x}_0) \in \mathbf{X}_1$ for $t \in [t_0, T]$. Let $\mathbf{Z} \subset \mathbf{X}_0$ be a positive Lebesgue measure set such that $s_T(t_0, \mathbf{Z}) \in \mathbf{X}_u$ for some $T > t_0$ and $s_t(t_0, \mathbf{Z}) \in \mathbf{X}_1$ for $t \in [t_0, T]$. Since

$\mathbf{Z} \subset \mathbf{X}_0$, utilizing Assumption 2.1 and from the construction of ρ , we have

$$\int_{s_T(t_0, \mathbf{Z})} \rho(T, \mathbf{x}) d\mathbf{x} = \theta \int_{s_T(t_0, \mathbf{Z})} \frac{1}{V_1(\mathbf{x})^\alpha} d\mathbf{x}, \quad (63)$$

$$\int_{\mathbf{Z}} \rho(t_0, \mathbf{x}) d\mathbf{x} = \int_{\mathbf{Z}} \frac{1}{V_1(\mathbf{x})^\alpha} d\mathbf{x}. \quad (64)$$

As \mathbf{Z} is assumed to be positive Lebesgue measure set, we have (64) greater than zero and since θ can be chosen to be arbitrary small but positive constant, we have (63)-(64) < 0 contradicting (62). This concludes the proof for avoidance and thus completes the proof of Theorem 2. ■

REFERENCES

- [1] H. Hewawasam, M. Y. Ibrahim, and G. K. Appuhamillage, "Past, present and future of path-planning algorithms for mobile robot navigation in dynamic environments," *IEEE Open Journal of the Industrial Electronics Society*, vol. 3, pp. 353–365, 2022.
- [2] A. V. Savkin, A. S. Matveev, M. Hoy, and C. Wang, *Safe robot navigation among moving and steady obstacles*. Butterworth-Heinemann, 2015.
- [3] M. Hoy, A. S. Matveev, and A. V. Savkin, "Algorithms for collision-free navigation of mobile robots in complex cluttered environments: a survey," *Robotica*, vol. 33, no. 3, pp. 463–497, 2015.
- [4] S. M. LaValle and J. J. Kuffner, "Rapidly-exploring random trees: Progress and prospects," *Algorithmic and Computational Robotics*, pp. 303–307, 2001.
- [5] D. Hsu, R. Kindel, J.-C. Latombe, and S. Rock, "Randomized kinodynamic motion planning with moving obstacles," *The International Journal of Robotics Research*, vol. 21, no. 3, pp. 233–255, 2002.
- [6] M. Likhachev, D. I. Ferguson, G. J. Gordon, A. Stentz, and S. Thrun, "Anytime dynamic A*: An anytime, replanning algorithm." in *ICAPS*, vol. 5, 2005, pp. 262–271.
- [7] O. Khatib, "Real-time obstacle avoidance for manipulators and mobile robots," *The International Journal of Robotics Research*, vol. 5, no. 1, pp. 90–98, 1986.
- [8] J. Borenstein, Y. Koren *et al.*, "The vector field histogram-fast obstacle avoidance for mobile robots," *IEEE Transactions on Robotics and Automation*, vol. 7, no. 3, pp. 278–288, 1991.
- [9] E. Rimon and D. Koditschek, "Exact robot navigation using artificial potential functions," *IEEE Transactions on Robotics and Automation*, vol. 8, no. 5, pp. 501–518, 1992.
- [10] C. Li and H. G. Tanner, "Navigation functions with time-varying destination manifolds in star worlds," *IEEE Transactions on Robotics*, vol. 35, no. 1, pp. 35–48, 2018.
- [11] C. Chen, C. Li, and H. G. Tanner, "Navigation functions with non-point destinations and moving obstacles," in *2020 American Control Conference (ACC)*. IEEE, 2020, pp. 2532–2537.
- [12] D. Helbing and P. Molnar, "Social force model for pedestrian dynamics," *Physical review E*, vol. 51, no. 5, p. 4282, 1995.
- [13] D. Helbing, I. Farkas, and T. Vicsek, "Simulating dynamical features of escape panic," *Nature*, vol. 407, no. 6803, pp. 487–490, 2000.
- [14] A. D. Ames, S. Coogan, M. Egerstedt, G. Notomista, K. Sreenath, and P. Tabuada, "Control barrier functions: Theory and applications," in *2019 18th European Control Conference (ECC)*. IEEE, 2019, pp. 3420–3431.
- [15] M. Igarashi, I. Tezuka, and H. Nakamura, "Time-varying control barrier function and its application to environment-adaptive human assist control," *IFAC-PapersOnLine*, vol. 52, no. 16, pp. 735–740, 2019.
- [16] V. Hamdipoor, N. Meskin, and C. G. Cassandras, "Safe control synthesis using environmentally robust control barrier functions," *European Journal of Control*, vol. 74, p. 100840, 2023.
- [17] M. Desai and A. Ghaffari, "Clf-cbf based quadratic programs for safe motion control of nonholonomic mobile robots in presence of moving obstacles," in *2022 IEEE/ASME International Conference on Advanced Intelligent Mechatronics (AIM)*. IEEE, 2022, pp. 16–21.
- [18] M. Jankovic, M. Santillo, and Y. Wang, "Multiagent systems with cbf-based controllers: Collision avoidance and liveness from instability," *IEEE Transactions on Control Systems Technology*, 2023.
- [19] M. Srinivasan, S. Coogan, and M. Egerstedt, "Control of multi-agent systems with finite time control barrier certificates and temporal logic," in *2018 IEEE Conference on Decision and Control (CDC)*. IEEE, 2018, pp. 1991–1996.
- [20] L. Lindemann and D. V. Dimarogonas, "Control barrier functions for multi-agent systems under conflicting local signal temporal logic tasks," *IEEE Control Systems Letters*, vol. 3, no. 3, pp. 757–762, 2019.
- [21] K. Garg, J. Usevitch, J. Breeden, M. Black, D. Agrawal, H. Parwana, and D. Panagou, "Advances in the theory of control barrier functions: Addressing practical challenges in safe control synthesis for autonomous and robotic systems," *Annual Reviews in Control*, vol. 57, p. 100945, 2024.
- [22] S. Bansal, M. Chen, S. Herbert, and C. J. Tomlin, "Hamilton-jacobi reachability: A brief overview and recent advances," in *2017 IEEE 56th Annual Conference on Decision and Control (CDC)*. IEEE, 2017, pp. 2242–2253.
- [23] N. Malone, H.-T. Chiang, K. Lesser, M. Oishi, and L. Tapia, "Hybrid dynamic moving obstacle avoidance using a stochastic reachable set-based potential field," *IEEE Transactions on Robotics*, vol. 33, no. 5, pp. 1124–1138, 2017.
- [24] Z. Zhou, J. Ding, H. Huang, R. Takei, and C. Tomlin, "Efficient path planning algorithms in reach-avoid problems," *Automatica*, vol. 89, pp. 28–36, 2018.
- [25] A. Bajcsy, S. Bansal, E. Bronstein, V. Tolani, and C. J. Tomlin, "An efficient reachability-based framework for provably safe autonomous navigation in unknown environments," in *2019 IEEE 58th Conference on Decision and Control (CDC)*. IEEE, 2019, pp. 1758–1765.
- [26] M. Doshi, M. Bhabra, M. Wiggert, C. J. Tomlin, and P. F. Lermusiaux, "Hamilton-jacobi multi-time reachability," in *2022 IEEE 61st Conference on Decision and Control (CDC)*. IEEE, 2022, pp. 2443–2450.
- [27] A. Rantzer and S. Prajna, "On analysis and synthesis of safe control laws," in *42nd Allerton Conference on Communication, Control, and Computing*, 2004.
- [28] D. V. Dimarogonas and K. J. Kyriakopoulos, "An application of rantzer's dual lyapunov theorem to decentralized formation stabilization," in *2007 European Control Conference (ECC)*. IEEE, 2007, pp. 882–888.
- [29] S. G. Loizou and A. Jadbabaie, "Density functions for navigation-function-based systems," *IEEE Transactions on Automatic Control*, vol. 53, no. 2, pp. 612–617, 2008.
- [30] B. Huang and U. Vaidya, "A convex approach to data-driven optimal control via perron–frobenius and koopman operators," *IEEE Transactions on Automatic Control*, vol. 67, no. 9, pp. 4778–4785, 2022.
- [31] U. Vaidya, "Optimal motion planning using navigation measure," *International Journal of Control*, vol. 91, no. 5, pp. 989–998, 2018.
- [32] H. Yu, J. Moyalan, U. Vaidya, and Y. Chen, "Data-driven optimal control of nonlinear dynamics under safety constraints," *IEEE Control Systems Letters*, vol. 6, pp. 2240–2245, 2022.
- [33] J. Moyalan, Y. Chen, and U. Vaidya, "Convex approach to data-driven off-road navigation via linear transfer operators," *IEEE Robotics and Automation Letters*, pp. 1–8, 2023.
- [34] J. Moyalan, A. Zheng, S. S. Narayanan, and U. Vaidya, "Off-road navigation of legged robots using linear transfer operators," *IFAC-PapersOnLine*, vol. 56, no. 3, pp. 613–618, 2023.
- [35] A. Zheng, S. S. Narayanan, and U. Vaidya, "Safe navigation using density functions," *IEEE Robotics and Automation Letters*, accepted, 2023.
- [36] L. W. Tu, "Manifolds," in *An Introduction to Manifolds*. Springer, 2011, pp. 47–83.
- [37] K. K. Hassan, "Nonlinear systems," *Departement of Electrical and computer Engineering, Michigan State University*, 2002.
- [38] S. S. Narayanan, A. Zheng, and U. Vaidya, "Safe motion planning for quadruped robots using density functions," in *2023 Indian Control Conference (ICC)*, accepted. IEEE, 2023.
- [39] J. Moyalan, S. S. Narayanan, A. Zheng, and U. Vaidya, "Synthesizing controller for safe navigation using control density function," in *2024 American Control Conference (ACC)*. IEEE, 2024, pp. 3397–3402.
- [40] I. Masubuchi and T. Kikuchi, "Lyapunov density criteria for time-varying and periodically time-varying nonlinear systems with converse results," *SIAM Journal on Control and Optimization*, vol. 59, no. 1, pp. 223–241, 2021.
- [41] P. Monzón, "Almost global stability of time-varying systems," in *Congresso Brasileiro de Automática, Bahia, Brasil, 2006*, 2006.
- [42] A. Rantzer, "A dual to Lyapunov's stability theorem," *Systems & Control Letters*, vol. 42, no. 3, pp. 161–168, 2001.
- [43] V. I. Arnold, *Ordinary differential equations*. Springer Science & Business Media, 1992.



Sriram S. K. S. Narayanan received his B.Tech degree in mechanical engineering from SAS-TRA University, India, in 2017, and his M.S. in mechanical engineering from the University of South Florida, Tampa, FL, USA in 2021. He is currently pursuing his Ph.D. in the Mechanical Engineering Department at Clemson University, Clemson, SC, USA. His current research interests include motion planning, optimal control, and model predictive control with applications to legged robots and autonomous vehicles.



Joseph Moyalan received his B.E. degree in electronics and telecommunication engineering from Mumbai University, India, in 2016, and his M. Tech. degree in electrical engineering (specialization in control systems) from Veermata Jijabai Technological Institute, Mumbai, India, in 2019. He completed his Ph.D. degree in the Mechanical Engineering Department at Clemson University, Clemson, SC, USA, in 2024. His current research interests include nonlinear optimal control, convex optimization, linear operators,

and data-driven control with application to vehicle autonomy.



Umesh Vaidya (M'07, SM'19) received the Ph.D. degree in mechanical engineering from the University of California at Santa Barbara, Santa Barbara, CA, in 2004. He was a Research Engineer at the United Technologies Research Center (UTRC), East Hartford, CT, USA. He is currently a professor in the Department of Mechanical Engineering at Clemson University, S.C., USA. Before joining Clemson University in 2019, he was a faculty member in the Department of Electrical and Computer Engineering at

Iowa State University from 2006. He received the National Science Foundation CAREER Award in 2012. His current research focuses on dynamical systems and control theory, with applications in power grids and robotics.